Analytical Methods

PAPER

View Article Online
View Journal | View Issue

Cite this: *Anal. Methods*, 2019, **11**, 296

Whole-cell biosensing by siderophore-based molecular recognition and localized surface plasmon resonance†

Jiayun Hu, [a] Manuka Ghosh, [b] Marvin J. Miller [a] and Paul W. Bohn *[ac]

Received 5th October 2018
Accepted 5th December 2018

DOI: 10.1039/c8ay02180e

rsc.li/methods

A siderophore-based active bacterial pull-down strategy was integrated in a localized surface plasmon resonance (LSPR) sensing platform and subsequently tested by detecting whole-cell *Acinetobacter baumannii*. The LSPR-based whole-cell sensing approach was previously demonstrated with aptamer-based molecular recognition motifs, and here it is extended to the powerful siderophore system, which exploits the natural bacterial need to sequester Fe(III). Specifically, a biscatecholate–monohydroxamate mixed ligand siderophore linked to a biotin *via* three polyethylene glycol repeating units was synthesized and immobilized on Au trigonal nanoprisms of an LSPR sensor. The resulting surface-confined biotinylated siderophore subsequently chelated Fe(III), forming a siderophore–Fe(III) complex which was shown to be competent to recognize *A. baumannii*. Target bacteria were captured and then detected by measuring wavelength shifts in the LSPR extinction spectrum. This siderophore pull-down LSPR biosensor approach is rapid (≤3 h detection) and sensitive – with a limit of detection (LOD) of 80 bacterial cells and a linear wavelength shift over the range 4×10^2 to 4×10^6 cfu mL^{-1}. As intended by design, the siderophore-based biosensor was selective for *A. baumannii* over *Pseudomonas aeruginosa*, *Escherichia coli*, and *Bacillus cereus*, and was stable in ambient conditions for up to 2 weeks.

Introduction

Biosensors, a central focus of efforts to produce advanced diagnostic tools, should exhibit rapid, sensitive, and cost-effective detection of specific targets.[1–3] More pointedly, label-free biosensors are favored in order to simplify operation. Localized surface plasmon resonance (LSPR) constitutes a powerful and popular label-free detection scheme which has attracted interest in the nanotechnology, bioanalytical, and medical diagnostics communities.[2,4–8] The key in LSPR sensing is its sensitivity to local refractive index change due to molecular adsorption. The direction (red- or blue-shift) and magnitude of the LSPR wavelength shift ($\Delta\lambda$) are affected by the molecular geometry and the packing density of the molecular adsorbates on the nanoparticles.[9] However, LSPR is non-specific; any type of molecular adsorption can generate an LSPR wavelength shift. To overcome this shortcoming a specific affinity reagent can be added to achieve target-specific detection. In this context, a key property of LSPR-based biosensors is the relatively small sensing volume, typically limited to within 10–100 nm of the surface,[6] although this can be tuned somewhat depending on the nanoparticle material and geometry. This characteristic can be used to advantage when the target completely fills the sensing volume due to its large size. For example, μm-sized bacterial cells can saturate the LSPR sensing volume yielding extraordinarily sensitive detection – down to a single bacterial cell.[10]

Despite these attractive features, there are relatively few examples of sensing biomedical targets with sizes in the μm range, such as whole-cell bacteria,[10–14] using LSPR spectroscopy.[15] Direct sensing of whole-cell bacteria could simplify detection protocols and shorten detection time by minimizing sample preparation (*e.g.*, purification, pre-concentration, cell culture), thus advancing bacterial infection diagnostics. In addition, LSPR-based pulldown assays allow temporal integration of bacterial load in very low concentration samples. To address this issue, our group has previously reported the development of an LSPR sensing platform and its application in the detection of whole-cell *Pseudomonas aeruginosa* using a *P. aeruginosa*-specific aptamer as an affinity reagent.[10] Here we report a strategic complement to aptamer-based LSPR sensors, by demonstrating a siderophore-based LSPR biosensor that is selective for *Acinetobacter baumannii*, a WHO priority pathogen.

[a]*Department of Chemistry and Biochemistry, University of Notre Dame, Notre Dame, Indiana 46556, USA. E-mail: pbohn@nd.edu; Fax: +1-574-631-8366; Tel: +1-574-631-1849*

[b]*Hsiri Therapeutics, Innovation Park, 1400 East Angela Boulevard, South Bend, Indiana 46617, USA*

[c]*Department of Chemical and Biomolecular Engineering, University of Notre Dame, Notre Dame, Indiana 46556, USA*

† Electronic supplementary information (ESI) available: Detailed experimental procedures, LC-MS characterization of biotinylated siderophore, LSPR wavelength shift after bacterial binding onto various sensor surface, and a Student's *t*-test showing siderophore selectivity. See DOI: 10.1039/c8ay02180e

Siderophores are low molecular weight (typically 500–1500 Da), high affinity (typically $K_f > 10^{30}$) metal-binding molecules produced by bacteria, fungi, and plants to scavenge environmental Fe(III) as an essential nutrient for their key biology functions.[16] Due to the low abundance of free Fe(III) in the environment (10^{-9} to 10^{-18} M),[17] siderophore iron acquisition mechanism is evolved such that, under starvation conditions (*i.e.*, intracellular Fe(III) concentration $\leq 10^{-6}$ M),[17] microbes will secrete one or more types of siderophores to sequester iron. Siderophore–Fe(III) complexes are actively recognized by microbes and transported into the microbial cytoplasm through the cell membrane utilizing various receptors, binding proteins, and transport proteins.[18] Compared to other common affinity reagents, siderophores offer desirable biological affinities to microbes, an active recognition mechanism, and selectivity to specific microbes.[19,20] In addition, they are "immutable ligands",[21] meaning that microbes are unlikely to develop mutations to prevent siderophore–Fe(III) complex intake, since this intake mechanism is essential for their survival.

A. baumannii is a particularly attractive target for the development of siderophore-based LSPR sensors. In 2017, the World Health Organization listed carbapenem-resistant strains of *A. baumannii* as top priority pathogens.[22–24] Additionally, the surface-immobilized version of a siderophore–Fe(III) complex recognition motif is used in a novel "Trojan Horse" configuration developed by Miller and coworkers.[20,25] Specifically, a biscatecholate–monohydroxamate mixed-type siderophore with three polyethylene glycol (PEG) repeating units linked to a biotin (Bt) was synthesized and integrated into an LSPR structure, Fig. 1(a), as an affinity reagent. This mixed ligand siderophore was chosen due to its high selectivity, as demonstrated by the remarkable and, by design, selective antibacterial potency against *A. baumannii* ATCC 17961 (minimum inhibitory concentration, MIC = 0.0078 μM) when it was conjugated with a carbacephalosporin β-lactam antibiotic[20] and subsequently to the large, usually Gram-positive-only antibiotic, daptomycin.[26] A biotin and three PEG repeating units were chosen to allow this siderophore to be immobilized onto an LSPR sensor surface *via* a biotin–NeutrAvidin linkage; thus rendering it competent to serve as a recognition agent after chelating subsequently added Fe(III).

The strategy involves the surface-confined siderophore–Fe(III) complex being actively and selectively recognized by the target microbe, and in the process of attempting to transport the siderophore–Fe(III) complex, the microbe becoming immobilized on the sensor surface. This, in turn, results in an altered refractive index of the medium above the LSPR substrate, thereby shifting the wavelength of the plasmon resonance ($\Delta\lambda$), which is measured before and after whole-cell bacterial capture. This siderophore-based LSPR sensing platform exhibits rapid detection (~3 h), selectivity for *A. baumannii* over *P. aeruginosa*, *Escherichia coli*, and *Bacillus cereus*, a linear LSPR response from 4×10^2 to 4×10^6 cfu mL^{-1} with a LOD of 80 *A. baumannii* cells, and up to 2 week shelf life in ambient conditions. Furthermore, we anticipate that this siderophore Trojan Horse sensing approach can be extended to a large variety of pathogens by

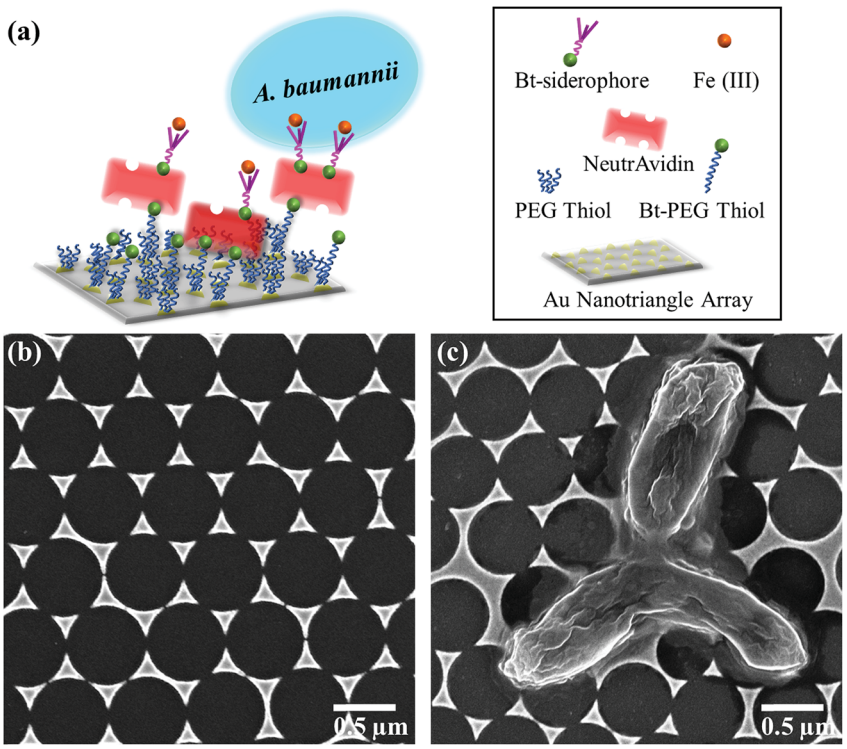

Fig. 1 (a) Schematic illustration of siderophore LSPR sensor chip design (left) with legend (right). (b, c) Representative SEM images of a bare sensor chip (b), and a sensor chip with captured *A. baumannii* cells (c). The trigonal prisms exhibit an in-plane width of 210.5 ± 9.1 nm, out-of-plane height of 47.6 ± 0.4 nm, and tip-to-tip distance of 121.3 ± 7.7 nm.

switching pathogen-specific siderophores. A number of sideromycins have been developed for different targets,[19,20,25–27] and all of these represent potential platforms for molecular recognition using this strategy.

Results and discussion

Siderophore synthesis and characterization

The key molecular recognition motif, a biscatecholate–monohydroxamate mixed ligand siderophore with three polyethylene glycol (PEG) repeating units linked to a biotin (Bt) (Bt–siderophore, conjugate **2**, Scheme 1) was synthesized as described in the ESI.† Briefly, the penta-acetyl-protected glutaryl siderophore **1** was converted to the corresponding chloroformate active ester by treatment with isobutyl chloroformate ($ClCO_2$i-Bu) in the presence of *N*-methylmorpholine (NMM) in anhydrous THF at 0 °C. The chloroformate ester formation was considered complete when TLC analysis showed complete consumption of the starting siderophore **1**. The PEG–Bt–siderophore, conjugate **2**, was obtained by coupling the mixed anhydride to the biotin–PEG–amine in aqueous bicarbonate, and purified using reverse phase chromatography C18 columns with a gradient of CH_3CN/H_2O. LC-MS analysis of the freshly synthesized biotinylated siderophore (ESI†) showed a major component and four minor components. The minor components resulted from the loss of one (M-OAc), two (M-2OAc), three (M-3OAc), and four (M-4OAc) acetyl groups. Just prior to bacterial binding experiments, the biotinylated siderophore in buffer was also characterized using LC-MS, Fig. S1,† revealing five components: (1) siderophore–Fe(III) complex without biotin, (2) and (3) two unknown iron complexes, (4) siderophore with neither biotin nor Fe(III), and (5) biotinylated siderophore without acetate. The Fe(III) observed in this analysis was from the environment, *e.g.*, buffer, since no iron was intentionally added to the sample. Among these five components, only the biotinylated siderophore (58% abundance) without acetate functions as a competent affinity reagent.

Sensor chip fabrication and sensor surface modification

A schematic illustration of the siderophore-based whole-cell LSPR sensor chip is shown in Fig. 1(a). The sensor chip, a microscope slide patterned with a hexagonal array of nanoscale Au trigonal prisms, was fabricated using nanosphere lithography (NSL).[28] A representative SEM image of a bare sensor chip is shown in Fig. 1(b). Detailed dimensional analysis of a typical sensor chip revealed in-plane width, 210.5 ± 9.1 nm, out-of-plane height, 47.6 ± 0.4 nm, and tip-to-tip distance, 121.3 ± 7.7 nm, of the trigonal prisms.[10]

The sensor surface was first modified with a mixture of Bt–PEG thiol (1000 Da) and PEG thiol (550 Da) in a 1 : 3 v/v ratio *via* self-assembly of the relevant organomercaptans on the nanoscale Au trigonal prisms. The PEG thiol, used to prevent nonspecific adsorption, has a shorter chain than the Bt–PEG thiol used to anchor subsequent surface immobilized moieties. The 1 : 3 ratio was determined previously to produce maximum bacterial binding on the sensor surface.[10] Tetrameric NeutrAvidin, with two biotin binding sites each on opposite sides of the protein,[29] was subsequently immobilized onto the biotin modified sensor surface *via* the strong non-covalent biotin–NeutrAvidin linkage; the affinity equilibrium constant, K_a, of NeutrAvidin for surface immobilized biotin is $\sim 5.5 \times 10^{11}$ M^{-1}.[30] NeutrAvidin, a deglycosylated avidin, was chosen over avidin and streptavidin due to its similar biotin-binding affinity,[31] more neutral isoelectric point (pI 6.3),[32] as well as its lower tendency for nonspecific binding.[33]

The Bt–siderophore, **2**, was subsequently immobilized onto NeutrAvidin modified sensor surface as an affinity reagent to pull-down *A. baumannii*. The same siderophore motif was previously conjugated to an antibiotic and exhibited selective inhibition of *A. baumannii* with strong potency (MIC = 0.0078

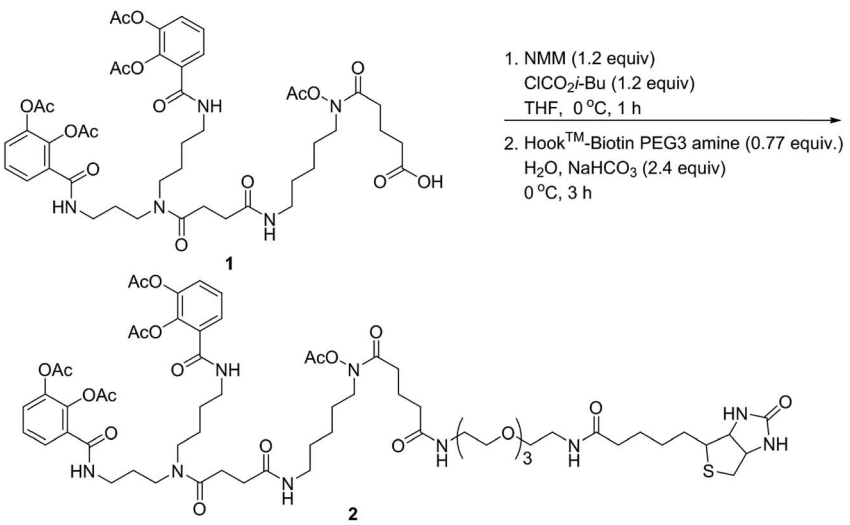

Scheme 1 Synthesis of biotinylated siderophore (Bt–siderophore, conjugate **2**) by coupling of the mixed anhydride of siderophore **1** and biotin PEG3 amine.

μM).[20] The demonstrated selectivity and potency recommend this siderophore as a promising affinity reagent. Siderophore-based recognition agents are also attractive, because bacteria are unlikely to evolve an alternative iron acquisition mechanism. However, in order to be recognized and utilized by bacteria, a siderophore has to chelate Fe(III) to form a siderophore–Fe(III) complex.[20] Thus, $Fe(acac)_3$ was subsequently introduced to the Bt–siderophore modified sensor surface as an additional iron source to saturate the surface-bound siderophores. Bacteria-containing solutions were then exposed to the siderophore–Fe(III) modified sensor surface. A representative SEM image of surface captured *A. baumannii* cells is shown in Fig. 1(c).

Characterization of *A. baumannii*-derived LSPR wavelength shift

LSPR spectroscopy was used to characterize surface modifications and bacterial binding. Representative near-infrared (NIR) extinction spectra of a bare sensor chip (curve 1, black), a modified sensor chip (curve 2, red), and a sensor chip with captured bacteria (curve 3, blue) are shown in Fig. 2. A typical unmodified sensor chip containing an array of nanoscale Au trigonal prisms exhibited an LSPR extinction maximum at 904.0 nm, which was red-shifted to 928.5 nm, *i.e.*, $\Delta\lambda = 24.5$ nm, after surface modification with Bt–PEG thiol/PEG thiol, NeutrAvidin, Bt–siderophore, and $Fe(acac)_3$. Once *A. baumannii* (4×10^6 cfu mL^{-1}) in 10 mM sodium phosphate solution was captured, the LSPR extinction maximum was further red-shifted to 941.5 nm, *i.e.*, $\Delta\lambda = 13.0$ nm. Despite differences in the initial LSPR extinction maximum among different unmodified sensor chips, red-shifts upon surface modification, as well as bacterial capture, were consistent between experiments.

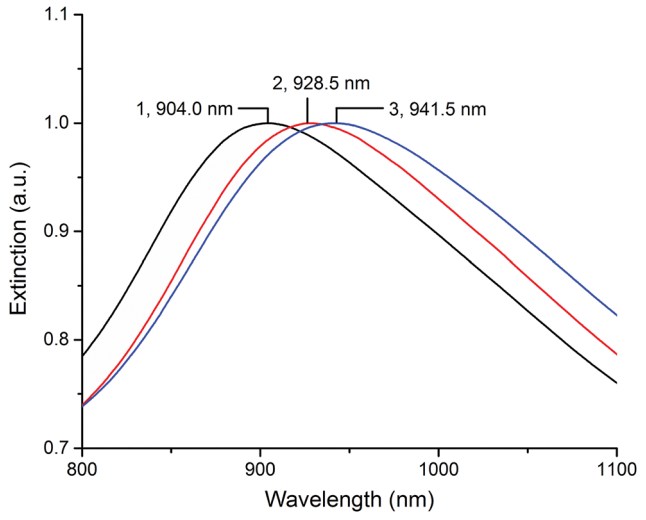

Fig. 2 Representative LSPR extinction spectra of nanoscale Au trigonal prism array (curve 1, black), the same array modified with Bt–PEG thiol/PEG thiol, NeutrAvidin, Bt–siderophore, and $Fe(acac)_3$ (curve 2, red), and after subsequent exposure to 4×10^6 cfu mL^{-1} *A. baumannii* in 10 mM sodium phosphate solution (curve 3, blue).

Control experiments

Various control experiments were carried out to investigate the role of both Bt–siderophore and externally added Fe(III) source in *A. baumannii* binding experiments. Fig. S2† shows a mean LSPR wavelength shift ($\Delta\lambda$) of -0.5 ± 2.6, 2.5 ± 4.3, and 7.4 ± 4.2 nm resulting from exposure of surfaces to *A. baumannii* (4×10^6 cfu mL^{-1}) in 10 mM sodium phosphate solution at three different surface modification stages: after addition of Bt–PEG thiol/PEG thiol and NeutrAvidin (black), after further modification with Bt–siderophore (red), and after exposure to $Fe(acac)_3$ (blue), respectively. Each of these conditions was tested using 12 to 16 individual sensor chips. Without Bt–siderophore and Fe(III), no *A. baumannii* statistically significant binding signal was observed, indicating a negligible amount of non-specific interaction between bacteria and the NeutrAvidin modified sensor surface. Immobilizing the Bt–siderophore, but without additional Fe(III), again produced a negligible wavelength shift. This observation suggests that even though surface confined Bt–siderophore may chelate trace amounts of adventitious environmental Fe(III), the resulting surface bound siderophore–Fe(III) complex is not sufficient to disrupt the measurement. Finally, a statistically significant *A. baumannii* binding signal was observed after supplying additional Fe(III) to the Bt–siderophore modified sensor surface in a 1 : 1 molar ratio. Interestingly, no additional binding resulted from a surface prepared with a 10-fold excess of $Fe(acac)_3$ (data not shown). Clearly, both Bt–siderophore and Fe(III) are essential for bacterial pull-down, and a 1 : 1 molar ratio of Bt–siderophore : $Fe(acac)_3$ was chosen for all following experiments.

Sensitivity

The sensitivity of the siderophore biosensor was investigated as a function of *A. baumannii* concentration ranging from 4×10^2 to 4×10^6 cfu mL^{-1} in 10 mM sodium phosphate solution, with each bacterial concentration being tested using 10 to 17 individual sensor chips. The mean LSPR wavelength shift ($\Delta\lambda$) was measured to be 2.9 ± 2.0 to 7.4 ± 4.2 nm across this range, with the control sample showing -0.9 ± 2.4 nm (Fig. 3). Fig. 3 inset shows that the siderophore biosensor exhibits a linear LSPR wavelength shift with log bacterial concentration. Using the Student's *t*-test, the difference between control (0 cfu mL^{-1}) and lowest test concentration (4×10^2 cfu mL^{-1}) establishes that the two can be discriminated at the 99.9% confidence level, thereby setting the LOD at 400 cfu mL^{-1}, which is equivalent to the active sensor area being exposed to 80 *A. baumannii* cells. However, because the actual number of cells resident on the sensor chip surface at the LOD condition is not known, 80 cells is an upper bound. The batch-to-batch variation in the production of sensor chips was shown to be minimal in a previous study.[10] However, there may be variations in the near-field distribution produced by the heterogeneity in the gold trigonal prism array. Thus, the measurement variability may arise from a combination of near-field and biological variation. The siderophore-based sensor characterized here exhibits a higher LOD (80 bacterial cells) than a similar LSPR biosensor

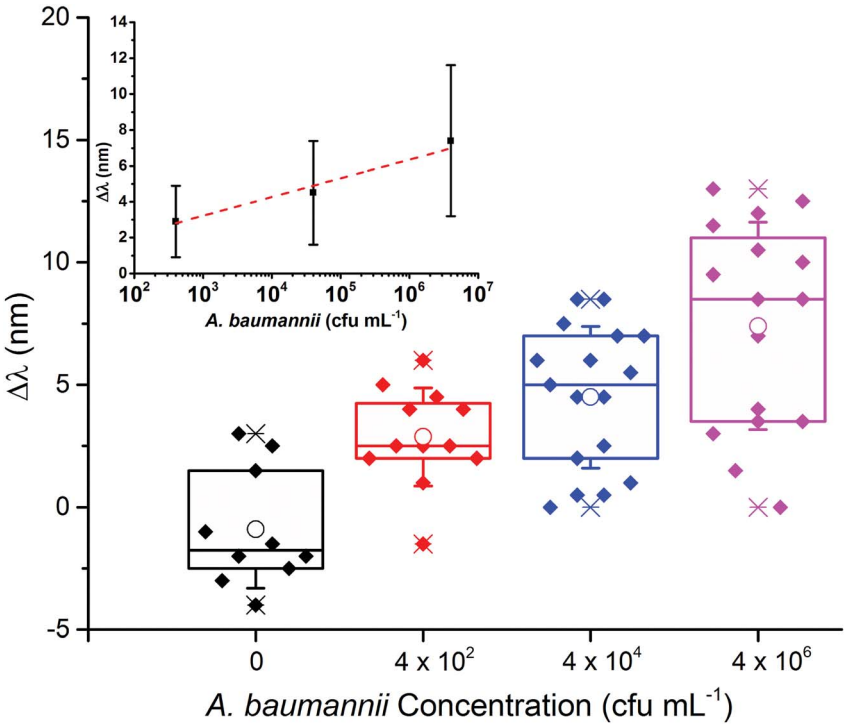

Fig. 3 A box and whisker plot demonstrating LSPR wavelength shift as a function of *A. baumannii* concentration. *A. baumannii* was suspended in 10 mM sodium phosphate solution. Each color represents a different bacterial concentration with 10 to 17 individual data points each (solid diamonds are results of individual experiments). The circle represents the mean of all data. The whiskers extend to ± one standard deviation. The lower, central, and upper box line represents 25th, 50th, and 75th percentile, respectively. Diagonal crosses (✗) represent the 1st and 99th percentiles. Insert shows a linear fit of LSPR wavelength shift *vs.* log bacterial concentration (red dash line), where the error bars represent the standard deviation of all data at a specific bacterial concentration.

for *P. aeruginosa* (LOD ~1 cell) employing an aptamer molecular recognition agent, which can plausibly be attributed to: (a) differing native affinities for the target; (b) differing availability of the transporter protein due to steric hindrance; (c) differing magnitude of the alteration in the near-surface refractive index profile, $n(z)$; and/or (d) impurities in the formulation, as indicated in the LC-MS analysis of the biotinylated siderophore (Fig. S1†). Nevertheless, compared to other biosensors targeting *A. baumannii*, the LOD of 400 cfu mL^{-1} compares quite favorably.[34]

Selectivity

Selective detection of the target analyte is a crucial figure-of-merit for biosensors. The selectivity of the siderophore biosensor was assessed against both Gram-negative (*Acinetobacter baumannii* ATCC 1796, *Pseudomonas aeruginosa* strain PAO1, *E. coli* DH5α) and Gram-positive (*Bacillus cereus*) bacteria. All four bacteria were grown in iron deficient media to mimic infection models that upregulate siderophore receptors, and bacterial concentrations were adjusted to ~10^7 cfu mL^{-1} in 10 mM sodium phosphate solution. Control experiments were carried out using 10 mM sodium phosphate solution without bacteria. *S. aureus*, another Gram-positive bacterium, was tested but is not included in this study, because it did not grow in the iron deficient media. Fig. 4 shows the LSPR wavelength shift corresponding to different bacterial species binding to the

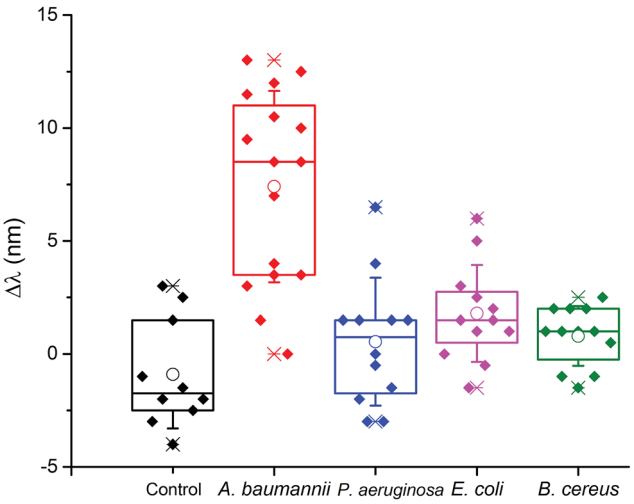

Fig. 4 A box and whisker plot showing LSPR wavelength shift corresponding to different bacteria binding to a *A. baumannii*-specific siderophore. A bacterial load of 10^7 cfu mL^{-1} in 10 mM sodium phosphate solution was tested in each case. Each color represents a control or a different bacterial sample with 10 to 16 individual data points (solid diamonds are results of individual experiments). The circle represents the mean of all data points. The whiskers extend to ± one standard deviation. The lower, central, and upper box line represents 25th, 50th, and 75th percentile, respectively. Diagonal crosses (✗) represent the 1st and 99th percentiles.

putative *A. baumannii*-selective sensor surface. Mean LSPR wavelength shifts of -0.9 ± 2.4, 7.4 ± 4.2, 0.5 ± 2.8, 1.8 ± 2.1, and 0.8 ± 1.3 nm were observed from the control, and from *A. baumannii*, *P. aeruginosa*, *E. coli*, and *B. cereus*, respectively. Application of Student's *t*-test shows there is a significant difference in LSPR wavelength shift between *A. baumannii* and control (no bacteria), *P. aeruginosa*, *E. coli*, and *B. cereus* at the 99.9% confidence level. These results demonstrate that the Bt–siderophore has a high affinity for *A. baumannii* and a negligible affinity towards *P. aeruginosa*, *E. coli*, and *B. cereus*. Our observations are consistent with previous findings in which biscatecholate–monohydroxamate mixed ligand sideromycins utilizing the carbacephalosporin β-lactam antibiotic loracarbef and the fluoroquinolone antibiotic ciprofloxacin were found to be selective for *A. baumannii*.[20] The demonstrated selectivity of the Bt–siderophore is a positive attribute of the siderophore recognition strategy and offers the possibility of identifying *A. baumannii* in a mixture of different bacteria.

Stability

Biosensor stability over a wide range of conditions (*e.g.*, temperature, humidity) is important for applications, especially in resource limited settings. To test the stability of the siderophore biosensor, sensor chips were stored in ambient conditions and their LSPR wavelength shifts were monitored every week for a month. Fig. 5 shows the LSPR wavelength difference between day 0 and day x, where $x = 7$, 14, 21, and 30 d. The observed mean LSPR wavelength shifts from 12 individual sensor chips were 0.1 ± 1.3, 1.5 ± 1.2, 2.4 ± 1.4, and 4.0 ± 1.8 nm after 7, 14, 21, and 30 days, respectively. The shifts at 7 and 14 days are not statistically significant relative to the control, indicating that siderophore–Fe(III) modified sensor chips are stable in ambient conditions for up to 2 weeks. The small, but monotonic, shift in extinction maximum likely arises from changes in composition and/or structure of the Au trigonal prisms, *e.g.* due to surface contamination.

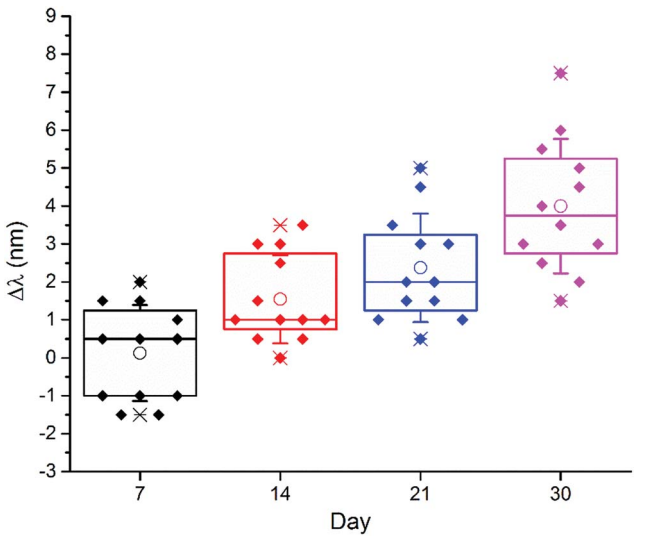

Fig. 5 The stability of modified sensor chips in ambient conditions was monitored using LSPR wavelength shift as a function of time. Each color represents the aging process of 12 individual Au trigonal nanoprism arrays modified with Bt–PEG thiol/PEG thiol, NeutrAvidin, Bt–siderophore, and $Fe(acac)_3$. The circle represents the mean of all data points. The whisker extends to ± one standard deviation. The lower, central, and upper box line represents 25th, 50th, and 75th percentile, respectively. Diagonal crosses (✗) represent the 1st and 99th percentiles.

Versatility

The utility of the whole-cell LSPR sensing approach was extended in this study using a novel siderophore-based Trojan Horse bacterial pull-down strategy. In previous work from this laboratory a *P. aeruginosa*-specific aptamer[35] was used as affinity reagent to selectively detect *P. aeruginosa*.[10] The surface-bound aptamer recognized and bound to an unspecified target on the bacterial outer cell membrane to pull-down and immobilize the bacteria. In the work here, we exploit the active recognition and iron transport mechanism, thereby hijacking the bacterial iron sequestration machinery in order to selectively pull-down *A. baumannii*. Thus, two different affinity reagent–analyte pairs, aptamer-*P. aeruginosa* and siderophore-*A. baumannii*, have now been demonstrated using the whole-cell LSPR pull-down strategy. Results from these two systems suggest that the whole-cell LSPR sensing platform is versatile and could be extended to a wide range of nm-scale to μm-scale targets (*e.g.*, bacteria, viruses, fungi) by exchanging target-specific affinity reagents. Thus, the whole-cell bacterial pull-down biosensor offers the opportunity to expand the diagnostic tool box for use against infectious agents.

Conclusions

The principal finding of this study is that the Trojan Horse strategy, which has been used effectively in sideromycins (siderophore–antibiotic conjugates), is also capable of capturing and immobilizing *A. baumannii* on a sensor surface, so that it can subsequently be readout by measuring the wavelength shift in the LSPR extinction spectrum. Importantly, this indicates that the cellular Fe–siderophore transport machinery is not compromised by surface-binding. Furthermore, the bacterial pull-down event is accompanied by a red-shift in the LSPR extinction maximum which exhibits a linear range from 4×10^2 to 4×10^6 cfu mL^{-1} with an LOD of 80 *A. baumannii* cells. As in the case of aptamer-based recognition of *P. aeruginosa*, the numerical LOD suggests a bacterial-derived collective resonance damping effect which enhances the LOD. Finally, the experiments presented here confirm the selectivity of the biscatecholate–monohydroxamate mixed ligand siderophore-based recognition element, as it was shown to be selective for *A. baumannii* over other Gram-negative (*P. aeruginosa*, *E. coli*) and Gram-positive (*B. cereus*) bacteria tested.

Further work to improve the whole-cell LSPR biosensor concentrates on critical application figures-of-merit. For example, the chip-to-chip reproducibility can be improved by enhancing the lithographic integrity and robustness of the NSL. Increasing the yield and stability of the Bt–siderophore will

improve the sensitivity and should also prolong the stability of the sensor chips. Moreover, the current detection time (~3 h) can be significantly shortened, if the bacterial inactivation step is not required. Finally, we note that the semi-quantitative operation demonstrated here is not needed in all applications. For example, simpler readout strategies can be employed when for threshold-sensitive sentinel applications, where a yes/no answer is all that is required.

Conflicts of interest

There are no conflicts to declare.

Acknowledgements

We acknowledge the National Institute of Allergies and Infectious Diseases (grant 1R01AI113219-01) for funding this work, the Notre Dame Nanofabrication Facility for supporting sensor chip fabrication, the Notre Dame Integrated Imaging Facility and the Notre Dame Materials Characterization Facility for supporting sensor chip characterization. We greatly appreciate the assistance of J. Shrout in providing supporting bacterial cell cultures, and W. Boggess and M. Lee for assisting in LC-MS analysis of the biotinylated siderophore.

References

1 A. Ahmed, J. V. Rushworth, N. A. Hirst and P. A. Millner, *Clin. Microbiol. Rev.*, 2014, **27**, 631–646.
2 J. Hu and P. W. Bohn, *Journal of Analysis and Testing*, 2017, **1**, 4.
3 N. Sanvicens, C. Pastells, N. Pascual and M.-P. Marco, *Trends Anal. Chem.*, 2009, **28**, 1243–1252.
4 A. J. Haes and R. P. Van Duyne, *Expert Rev. Mol. Diagn.*, 2004, **4**, 527–537.
5 K. A. Willets and R. P. V. Duyne, *Annu. Rev. Phys. Chem.*, 2007, **58**, 267–297.
6 K. M. Mayer and J. H. Hafner, *Chem. Rev.*, 2011, **111**, 3828–3857.
7 J.-F. Masson, *ACS Sens.*, 2017, **2**, 16–30.
8 H. Yu, K. Kim, K. Ma, W. Lee, J.-W. Choi, C.-O. Yun and D. Kim, *Biosens. Bioelectron.*, 2013, **41**, 249–255.
9 A. J. Haes, W. P. Hall, L. Chang, W. L. Klein and R. P. Van Duyne, *Nano Lett.*, 2004, **4**, 1029–1034.
10 J. Hu, K. Fu and P. W. Bohn, *Anal. Chem.*, 2018, **90**, 2326–2332.
11 S. M. Yoo, D.-K. Kim and S. Y. Lee, *Talanta*, 2015, **132**, 112–117.
12 J. Fu, B. Park and Y. Zhao, *Sens. Actuators, B*, 2009, **141**, 276–283.
13 S. Y. Oh, N. S. Heo, S. Shukla, H.-J. Cho, A. T. E. Vilian, J. Kim, S. Y. Lee, Y.-K. Han, S. M. Yoo and Y. S. Huh, *Sci. Rep.*, 2017, **7**, 10130.
14 N. A. Cinel, S. Butun and E. Ozbay, *Opt. Express*, 2012, **20**, 2587–2597.
15 P. J. Vikesland and K. R. Wigginton, *Environ. Sci. Technol.*, 2010, **44**, 3656–3669.
16 R. C. Hider and X. Kong, *Nat. Prod. Rep.*, 2010, **27**, 637–657.
17 M. Miethke and M. A. Marahiel, *Microbiol. Mol. Biol. Rev.*, 2007, **71**, 413–451.
18 M. Sandy and A. Butler, *Chem. Rev.*, 2009, **109**, 4580–4595.
19 T. A. Wencewicz, T. E. Long, U. Möllmann and M. J. Miller, *Bioconjugate Chem.*, 2013, **24**, 473–486.
20 T. A. Wencewicz and M. J. Miller, *J. Med. Chem.*, 2013, **56**, 4044–4052.
21 D. D. Doorneweerd, W. A. Henne, R. G. Reifenberger and P. S. Low, *Langmuir*, 2010, **26**, 15424–15429.
22 *Antibiotic Resistance Threats in the United States, 2013*, Centers for Disease Control and Prevention, Atlanta, GA, 2013, https://www.cdc.gov/drugresistance/threat-report-2013/pdf/ar-threats-2013-508.pdf, accessed June 12, 2018.
23 *Antimicrobial Resistance*, World Health Organization, Geneva, 2018, http://www.who.int/news-room/fact-sheets/detail/antimicrobial-resistance, accessed May 25, 2018.
24 *WHO Publishes List of Bacteria For Which New Antibiotics Are Urgently Needed*, World Health Organization, Geneva, 2017, http://www.who.int/en/news-room/detail/27-02-2017-who-publishes-list-of-bacteria-for-which-new-antibiotics-are-urgently-needed, accessed May 25, 2018.
25 M. J. Miller, A. J. Walz, H. Zhu, C. Wu, G. Moraski, U. Möllmann, E. M. Tristani, A. L. Crumbliss, M. T. Ferdig, L. Checkley, R. L. Edwards and H. I. Boshoff, *J. Am. Chem. Soc.*, 2011, **133**, 2076–2079.
26 M. Ghosh, P. A. Miller, U. Möllmann, W. D. Claypool, V. A. Schroeder, W. R. Wolter, M. Suckow, H. Yu, S. Li, W. Huang, J. Zajicek and M. J. Miller, *J. Med. Chem.*, 2017, **60**, 4577–4583.
27 R. Liu, P. A. Miller, S. B. Vakulenko, N. K. Stewart, W. C. Boggess and M. J. Miller, *J. Med. Chem.*, 2018, **61**, 3845–3854.
28 J. C. Hulteen and R. P. Van Duyne, *J. Vac. Sci. Technol.*, 1995, **13**, 1553–1558.
29 M. Wilchek and E. A. Bayer, in *Methods in Enzymology*, ed. M.Wilchek and E. A.Bayer, Academic Press, Cambridge, MA, 1990, vol. 184, pp. 5–13.
30 J. R. Wayment and J. M. Harris, *Anal. Chem.*, 2009, **81**, 336–342.
31 Y. Hiller, J. M. Gershoni, E. A. Bayer and M. Wilchek, *Biochem. J.*, 1987, **248**, 167–171.
32 Instructions for NeutrAvidin Biotin-Binding Protein, https://assets.thermofisher.com/TFS-Assets/LSG/manuals/MAN0011245_NeutrAvidin_Biotin_BindProtein_UG.pdf, accessed June 11, 2018.
33 Y. Hiller, E. A. Bayer and M. Wilchek, in *Methods in Enzymology*, ed. M.Wilchek and E. A.Bayer, Academic Press, Cambridge, MA, 1990, vol. 184, pp. 68–70.
34 O. M. Pavlyuk and O. N. Ruiz, *Energy Fuels*, 2017, **31**, 3747–3758.
35 K.-Y. Wang, Y.-L. Zeng, X.-Y. Yang, W.-B. Li and X.-P. Lan, *Eur. J. Clin. Microbiol. Infect. Dis.*, 2011, **30**, 273–278.

